

Vi-Liquid: Unknown Liquid Identification with Your Smartphone Vibration

Yongzhi Huang, Kaixin Chen, Yandao Huang, Lu Wang, Kaishun Wu*

{huangyongzhi,2017133035,2016040084}@email.szu.edu.cn,{wanglu,wu}@szu.edu.cn

CSSE, Shenzhen University, Shenzhen, GD CN

ABSTRACT

Traditional liquid identification instruments are often unavailable to the general public. This paper shows the feasibility of identifying unknown liquids with commercial lightweight devices, such as a smartphone. The wisdom arises from the fact that different liquid molecules have various viscosity coefficients, so they need to overcome dissimilitude energy barriers during relative motion. With this intuition in mind, we introduce a novel model that measures liquids' viscosity based on active vibration. Yet, it is challenging to build up a robust system utilizing the built-in accelerometer in smartphones. Practical issues include under-sampling, self-interference, and volume change impact. Instead of machine learning, we tackle these issues through multiple signal processing stages to reconstruct the original signals and cancel out the interference. Our approach could achieve the liquid viscosity estimates with a mean relative error of 2.9% and distinguish 30 kinds of liquid with an average accuracy of 95.47%.

CCS CONCEPTS

- Human-centered computing → Smartphones; Mobile computing: Ubiquitous and mobile computing design and evaluation methods;
- Applied computing → Physics.

KEYWORDS

Liquid; Viscosity Coefficient; Identification; Mobile Sensing; Ubiquitous Computing

ACM Reference Format:

Yongzhi Huang, Kaixin Chen, Yandao Huang, Lu Wang, Kaishun Wu. 2021. Vi-Liquid: Unknown Liquid Identification with Your Smartphone Vibration. In *The 27th Annual International Conference On Mobile Computing And Networking (ACM MobiCom '21), October 25–29, 2021, New Orleans, LA, USA*. ACM, New York, NY, USA, 14 pages. <https://doi.org/10.1145/3447993.3448621>

1 INTRODUCTION

Motivation: Liquid testing has recently attracted significant interest. Researches have led to solutions that deliver inexpensive and ubiquitous liquid testing outside the lab environment[11, 17, 18, 28,

*Kaishun Wu is the corresponding author

Permission to make digital or hard copies of all or part of this work for personal or classroom use is granted without fee provided that copies are not made or distributed for profit or commercial advantage and that copies bear this notice and the full citation on the first page. Copyrights for components of this work owned by others than the author(s) must be honored. Abstracting with credit is permitted. To copy otherwise, or republish, to post on servers or to redistribute to lists, requires prior specific permission and/or a fee. Request permissions from permissions@acm.org.

ACM MobiCom '21, October 25–29, 2021, New Orleans, LA, USA

© 2021 Copyright held by the owner/author(s). Publication rights licensed to ACM.

ACM ISBN 978-1-4503-8342-4/21/10.

<https://doi.org/10.1145/3447993.3448621>

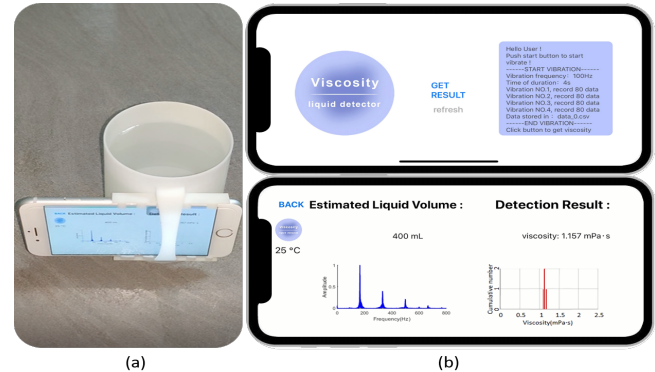


Figure 1: (a) Using iPhone 7 to detect liquid. (b) The user interface.

35]. The potential application scenarios of ubiquitous liquid testing range from safety inspection in public transportation, identification of fake luxury perfume, detection of water contamination in countries with limited sanitary water facilities, monitoring daily nutrition intake from drinks, in-home urine testing to track disease progression, etc.

Unfortunately, the proposed liquid testing systems require specialized external devices like RFID readers [17, 35], photodiodes [18], ultra-wideband (UWB) units [11], and piezoelectric sensors [28]. The difficulty in deploying and using for the general public prevents those systems from penetrating our daily life. CapCam [42] is the first and only work that measures liquids' surface tension only with a smartphone. However, it requires prior knowledge about the transparent liquid (such as measuring the density of liquids in advance), and thus it is unable to identify unknown liquids.

In this paper, we try to ask whether we can identify unknown liquids (the liquid in the container without information leak out) with a commercial device, such as a smartphone. To answer this question, we need to find a novel property, and it is unique to different liquids and accessible to smartphones. Fortunately, we found viscosity, an inherent property of liquid. Viscosity describes the resistance force generated by the relative movement of liquid molecules. Different liquid molecules have various viscosity coefficients, so they need to overcome different energy barriers during relative motion. If we can measure the liquid viscosity, we can identify the liquid type and analyze the liquid concentration. However, conventional viscosity testing instruments [6, 10, 16, 29, 31, 33] are expensive and invasive. It will also contaminate the liquid when measuring the viscosity with a rotatable probe. How to measure the liquid viscosity with a smartphone remains unknown.

Our approach: In this paper, we present Vi-Liquid¹, a lightweight smartphone application that measures the liquid viscosity for unknown liquid testing by leveraging only a built-in vibro-motor and an accelerometer. As shown in Figure 1, to measure the liquid viscosity, the user attaches the smartphone to the container and activates the app. Afterwards, Vi-Liquid generates active vibration signals through the built-in vibro-motor and collects the reflected vibration signals using a built-in accelerometer. The signals are feed into our proposed Vibration-Viscosity model to calculate the viscosity result. The critical insight behind Vi-Liquid is that the liquid will create a viscosity-related resistance force when giving an external activation, as the active vibration from a vibro-motor. We can calculate the viscosity by analyzing the received vibration signal affected by this resistance force.

Challenges and Solutions: However, it is non-trivial to measure the liquid viscosity using active vibration signals generated from a smartphone. To ensure accuracy, reliability, and usability, we have to address three challenges: (i) First, it is unclear how to calculate the viscosity by leveraging the influence and physical characters from active vibration to the liquid. It is necessary to build up a model that represents the relationship between vibration signals and liquid viscosity. (ii) Second, the intrinsic restriction of hardware settings regarding vibro-motor and accelerometer in smartphones poses another challenge to the vibration signal's design and analysis. As the maximum sampling rate through API is limited to 100Hz in the COTS smartphones, the sampled signals are distorted and causing considerable measurement errors. (iii) Third, in practical usage, we encounter two main interferences. One comes from the self-interference. When the vibration signal transmits directly to the accelerometer, it overwhelms the low SNR signal reflected from the target liquid. The other is that the change of liquid volume results in different signal patterns, making the viscosity measurement inconsistent even if they are the same liquid.

To address the first challenge, we build the kinematics equation of single-degree-of-freedom to link the liquid viscosity, the *shearing force* from liquid to the container, and the vibration signal together. We observe that the amplitude of the reflected vibration signal in *steady-state* is affected by the *shearing force*, and the attenuation in *decaying-state* is dominant by the viscosity-related damping coefficient. Then we verify the proposed model with several experiments in the feasibility study. The second challenge is to solve the system safety mechanism on sampling restriction. We need to restore the undersampled signal, termed *Supersampling Rate Reconstruction*. This algorithm utilizes the phase shift of the vibration signal to combine the sample points of multiple periods into one period. We further improve the restored signal by applying *orthogonal matching pursuit* to recover the complete signal and enhanced the processing efficiency. To deal with the third challenge, we subtract the pre-recorded straight path signals from the received vibration signals to cancel the straight interference. In the next stage, we set a series of weights for each liquid volume to calibrate the amplitude affected by the liquid's volume change.

Summary of Experiment Results: Vi-Liquid has high accuracy for viscosity measurement, and the mean relative error for 30 kinds of liquids is only 2.9%. Within this error range, Vi-Liquid can also

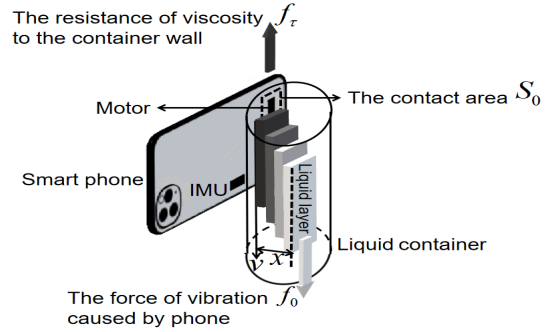


Figure 2: The detecting model of Vi-Liquid.

identify liquids with an average accuracy of 95.47%, including highly similar beverages, such as Coca-Cola and Pepsi. It can also accurately distinguish liquids based on the content of different mass concentrations of salt, sugar, and fat. Distinguish pollution water has only 2.56% mean relative error. Furthermore, Vi-Liquid identifies uric acid and urine protein in urine with errors of 1.15 mg/100mL and 0.20 mg/100mL, respectively. The urine test function with this error range can be used as *at-home diagnostic monitor* and *health admonishes* to identify common asymptomatic diseases, such as nephritis, with the uric acid concentration higher than 60 mg/100mL [15] and protein concentration higher than 3 mg/100mL complication [36]. Our error in identifying alcohol concentration is only 1.38% by mass, which can well allow users to avoid the health risks caused by alcohol.

Contributions: The main contributions in Vi-Liquid summarise as follows:

- We propose Vi-Liquid to identify unknown liquid based on viscosity using smartphone-generated vibration, which is the first work that identifies unknown liquid only with a smartphone to the best of our knowledge. Vi-Liquid can detect water contamination, monitor alcohol intake, and measure uric acid and protein concentration in urine.
- We establish a viscosity measurement model using vibration signals and verify its feasibility. We propose multiple stages of approaches to overcome several practical issues and build up a robust system.
- We implement Vi-Liquid as an efficient application running on a COTS iOS smartphone and validate its performance through comprehensive experiments. On average, our system yields a viscosity estimation error of 2.9% compared to that of 1% obtained by the high-cost viscosity instrument.

The rest of the paper is organized as follows: In Section 2, we detail why vibro-motor and accelerometer modules can indicate the feature of liquid viscosity from theoretical models. We give the feasibility study by analyzing the received vibration readings in Section 3. After the system overview in Section 4, we introduce the system design and illustrate how we address the challenges when migrating the system to a smartphone in Section 5. In Section 6, we present several case studies to evaluate our system performance on a smartphone. We discuss the related work in Section 7. Finally, we give the conclusion and future work in Section 8.

¹<https://youtu.be/Gpt5eJXHFBQ>

2 VIBRATION MODEL FOR VISCOSITY MEASUREMENT

In this section, we will introduce the theoretical models for liquid detection.

2.1 Liquid Viscosity and the Shearing Force

Viscosity is an essential physical attribute of liquids. When liquid molecules move in space, they have to overcome the friction caused by the relative motion between them, which accounts for liquid molecules' viscosity in the microscopic [13, 14]. The higher the force between molecules, the more significant the energy barrier. The viscosity η can be expressed as

$$\eta = \frac{hN}{V} e^{-\frac{\Delta G}{RTemperature}} \quad (1)$$

where V is the molar volume of the molecule, ΔG is the Gibbs energy change of the molecule, *Temperature* is the temperature, h , N and R are Prang Gram constant, Avogadro constant, and Boltzmann constant, respectively. We assume the indoor temperature is stable and regard *Temperature* as a constant. Different kinds of the molecule have diverse Gibbs energy, which indicates the energy-consuming for each molecule's unit distance movement. The Gibbs energy change and molar volume of the molecule are various for each kind of molecule. Therefore, the liquids can be distinguished by their viscosity. For instance, the viscosity of distilled water, ethyl alcohol, and honey are 1 cP, 1.2 cP, and 3000 cP² at 20 °C.

In macroscopic observations [3], a liquid's viscosity characterizes the frictional force between different liquid layers, as shown in Fig. 2. Given an external force f_0 , the resistance force between liquid and container is a shearing force f_τ that can be modeled as follows:

$$f_\tau = \eta S_0 \frac{v}{x} \quad (2)$$

where S_0 is the contact area between the liquid layer and container, and v is the movement speed of the liquid. x refers to the layer depth of moving liquid. Given a certain liquid volume and vibration, the S_0 , v , and x can be considered as constants. Thus, we can measure the viscosity η by leveraging its linear relationship with f_τ .

2.2 Viscosity Calculation leveraging Vibration

However, it is still non-trivial to measure the viscosity using a smartphone after learning the theory above. In this section, we illustrate the viscosity calculation model using a smartphone. During the measurement, the built-in vibro-motor generates vibration actively outside the liquid container. Due to the characteristic of liquid viscosity, a resistance force (i.e., the shearing force) will occur when the liquid flow. Our purpose is to detect this shearing force using the accelerometer, and what's more, calculate the viscosity.

Specifically, we can separate the vibration into three states: the transient, the steady, and the decaying-state. We eliminate the vibration signals in transient-state, which last a short time in the beginning since it is highly dynamic and intractable to model. When it comes to steady-state, we consider the vibrated liquid layer as a study object and model a spring-mass-damper model of single-degree-of-freedom. Given the constant external force f_0 caused by



Figure 3: Confirmatory experiments were set up by separate motor, accelerometer, container and alternating current power supply.

the motor as a sinusoidal vibration, we have:

$$m \frac{d^2x}{dt^2} + \beta \frac{dx}{dt} + kx = (f_0 - f_\tau) \sin(\omega t) \quad (3)$$

Among them, m is the mass of the vibrated liquid layer (known as the Stokes boundary layer [36]). β is a damping coefficient affected by viscosity. The elastic coefficient k is mainly affected by the container, and it is a constant that we can obtain by looking up the datasheet [32]. ω is the angular frequency of the vibro-motor. The particular solution of the Differential Equation (3) is:

$$x_{vib} = \frac{f_0 - f_\tau}{\sqrt{(k - \omega^2 m)^2 + (\beta \omega)^2}} \sin(\omega t - \phi) \quad (4)$$

where $\phi = \arctan(\frac{\beta \omega}{k - m\omega^2})$. Owing to the frequency and intensity of the smartphone driving signal is constant, ω and f_0 are regarded as constant. Hence, we can estimate the viscosity from the maximum amplitude of the vibration A , without tracking the vibration trajectory.

$$A = \frac{f_0 - f_\tau}{\sqrt{(k - \omega^2 m)^2 + (\beta \omega)^2}} \quad (5)$$

Next, we focus on the viscosity-related damping coefficient β . When the external force induced by the motor pause, the system turns to decaying-state, where the vibration of liquid gradually decays and then stops. The equation of motion in decaying-state is:

$$m \frac{d^2x}{dt^2} + \beta \frac{dx}{dt} + kx = 0 \quad (6)$$

where the general solution to the equation is:

$$x_{decay} = A e^{-\frac{\beta}{2m}t} \sin\left(\sqrt{\frac{k}{m}} \sqrt{1 - \left(\frac{\beta}{2\sqrt{km}}\right)^2} t + \theta\right) \quad (7)$$

As the amplitude attenuating constantly, we can record the amplitude of A_i in the same period T , and calculate the decaying factor Λ as:

$$\Lambda = \frac{x_{decay}(t)}{x_{decay}(t+T)} = e^{T \cdot \frac{\beta}{2m}} \quad (8)$$

Therefore, we can be used the attenuation of the amplitude in adjacent periods to assess the β . Note that the m is a constant that can calibrate in advanced. Specifically, when the motor is paused, we apply the peak amplitude values in adjacent periods to calculate the decaying factor Λ and eliminate noise by averaging the results.

Next, we can calculate the resistance of f_τ leveraging the transient-state amplitude A . Finally, we can estimate the viscosity η based on the shearing force f_τ from the target liquid.

²cP is a unit of viscosity, which can be also written as mPa · s

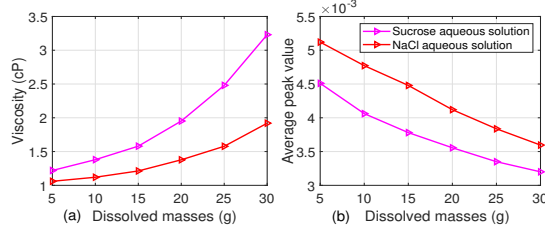


Figure 4: Dissolving different mass of sucrose and NaCl in solution. (a) Change of viscosity. (b) Change of average peak value.

3 FEASIBILITY STUDY

This section will verify the proposed model and demonstrate the feasibility of applying the standalone vibro-motor and accelerometer to measure liquid viscosity.

3.1 Experimental Setup

We utilized a 3D printer (Form 3) to print a 500 mL of tableware resin cup with two side slots at the position of 250 ml metric value. The vibro-motor (iPhone 7 Taptic Engine) and 3-axis accelerometer (BMI160) were deployed inside the slots, as shown in Figure 3. We set the vibration frequency as 167 Hz, which is in line with the vibration frequency in the mobile phone we used (i.e., iPhone 7). In the data collection part, we set the accelerometer's sampling rate as 1600 Hz for high data resolution. We measured the viscosity through the shearing force, so only X-axis data are used for analysis. For the ground truth, we utilized a rotatory viscometer ATAGO – VISCOTM 895 to measure the liquid viscosity. It provides a measurement range from 1 to 3.5×10^8 cP with a resolution of 0.01 cP. The ground truth measurement has a relative error of 1%. We run all the experiments in a laboratory with a stable room temperature at 25°C. Unless otherwise specified, the following experiments are conducted under the setting discussed above.

3.2 The Viscosity Uniqueness of Liquids

We first explore how different viscosity coefficients affect the vibration signals we received.

To control the influence of the two variables: mass and volume, making the liquid viscosity the only variable, we need to find two suitable liquids. The liquids should meet the condition that the volume growth rate is the same, but the viscosity growth rate is different when adding the same mass of the solutes. For instance, when we added dissimilitude solutes with the equivalent mass into the containers filling them with the same volume water, both liquids have the same volume increase, but diverse viscosity increases.

In our pilot study, we iterated the setting and found that, at 18°C, the sucrose aqueous solution and the NaCl aqueous solution meet the experimental conditions.

We constantly dissolved sucrose and NaCl to 450 mL of water and recorded their viscosity and vibration readings. From the results plotted in Figure 4, we had following findings: From Figure 4(a), we could see that the higher the liquid concentration is, the higher the liquid viscosity we have; two liquids of the same volume and mass have distinctive viscosity coefficients. We noticed that, in Figure 4(b), the average peak value varies considerably even though the smallest viscosity gap is only 0.16 cP when the dissolved mass is 5

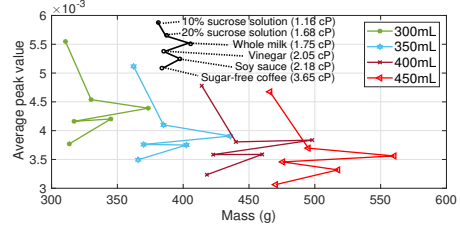


Figure 5: The distribution of different volumes of liquid in the mass-amplitude graph.

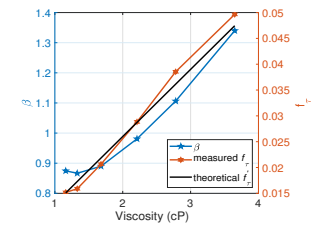


Figure 6: The measured value β , f_τ and the theoretical f_τ .

g, which interpret the viscosity will cause significant attenuation to the vibration. However, based on the results in Figure 4(b), the average peak value is related to both viscosity and mass of liquid. We still can not conclude that the peak value reveals the unique viscosity of the liquid. Therefore, we will further verify the findings in the next experiment.

3.3 The Impact of Mass

Can the mass affect the vibration signal? According to the model above, the liquid's mass is not an effect variable as it is the Stokes boundary layer mass, which is a constant. Accordingly, we will prove that the liquid's mass is independent in the following experiments. We prepared six liquids of different viscosity (10% and 20% sucrose solutions, whole milk, vinegar, soy sauce, and sugar-free coffee) in four volumes ($6 \times 4 = 24$ liquid samples in total). We recorded the average peak values of these samples' amplitude and mass and the results is demonstrated in Figure 5.

We found that the mass variation does not correlate to the amplitude variation. Taking the green line (300 mL) as an example, we could observe that the whole milk with more mass results in a smaller amplitude than sucrose solution. It seems to be counter-intuitive. In fact, in fluid mechanics, this principle is called the Stokes boundary layer theory. We attached the sensor to the container's wall instead of the bottom, which was not disturbed by mass. According to the Stokes boundary theory, the container wall's vibration amplitude is tiny, so the affected liquid only a thin layer near the boundary. Compared with the density, the liquid is more affected by the surface area. Therefore, the variable mass refers to the liquid layer, and we can regard it as a constant.

3.4 The Volume interference

On the other hand, the volume change has a more significant influence on the amplitude for the same liquids. Because the increase in liquid volume results in a larger contact area S_0 . According to Equation 2 and 5, we have a larger shearing force f_τ , which leads to a smaller amplitude A . We detail the design of a calibration scheme for tackling this impact in Section 5.

The change of volume will also cause disturbance to vibration.

We use the viscometer to measure six groups of sucrose solutions with mass concentrations of 10%, 15%, 20%, 25%, 30%, and 35%. Their viscosity are 1.16 cP, 1.33 cP, 1.68 cP, 2.21 cP, 2.78 cP, and 3.65 cP, respectively. In order to verify the volume interference, we filled the container with different volumes of the sucrose solutions, then detected changes in amplitude from 100 mL to 500 mL. We measured fifty sets of data every 50 mL and calculated the

average peak value of the amplitude. Through measurement, we found that although the volume has a negative correlation with the amplitude, the change interval is not proportional. As shown in Figure 7, when the volume increases, the decay rate of amplitude gradually decreases ($a > c$), and the decay is the same ($a = b$) although the viscosity is different.

3.5 Attenuation in Decaying-state

In this section, we explore the attenuation characteristic in liquids of the same volume but different viscosity in the decaying-state. We filled with 400 mL sucrose solution in different concentrations (10%, 15%, 20%, 25%, 30%, and 35%). As shown in Figure 8, when the vibration stops, the vibration gradually decays. It shows that the higher the viscosity of the liquid, the faster the vibration decays.

We can get the mean value of decaying factor $\bar{\Lambda}$ by calculating the ratio of adjacent peaks and then solve β according to Equation 8. With β , we can further derive f_r and then to estimate η . As shown in Figure 6, the f_r we calculated is very close to the theoretical f'_r , and the mean relative error is 4.57%.

3.6 The Impact of Container

In this section, we explore the interference brought by the container. We designed the experiments using containers of different materials (i.e., resin, plastic, and ceramic) in the same size. The containers were placed on the same table, filled with 400 mL sucrose solution in different concentrations, 10%, 15%, 20%, 25%, 30%, and 35%. We further explored the influence of container thickness, and utilized three different thickness resin containers (1 mm, 2 mm and 3 mm), and recorded the same volume and concentration sucrose solutions mentioned above. We recorded the relationship between the average amplitude of the accelerometer and the viscosity in Figure 9.

Through experiments, we found that the container's wall material and thickness impact on the amplitude value. Different effects also occur on the curve slope when the container's wall material and thickness change. The result verifies that no matter how the container's wall shape and material change, as long as we can get the elastic coefficient constant value k of the container wall, we can eliminate the interference from different containers.

4 SYSTEM OVERVIEW

Vi-Liquid is mainly composed of five modules, as shown in Figure 10.

Parameter Calibration Module: Considering the errors between different mobile phones and containers, Vi-Liquid needs to calibrate and determine the parameters. By testing several viscosities known liquids, Vi-Liquid will calibrate the model's uncertain parameters through the known information. After the initial calibration, the model is ready for the testing of liquid.

Motion Detection Module: Considering the device's motion will interfere with the detected signal and cause misjudgement, we need to prevent the motion state when identifying the liquid. Therefore, we need to use Apple's motion recognition API "CMMotionActivityManager" [1] as the motion detection interface. This module divides the parameters returned by the API into two statuses, stable and unstable. When the module finds out the device is under an

unstable scenario, the system would stop the detection process and wait until turning better.

Signal Reconstruction Module: By changing the interval time, Vi-Liquid applies *Supersampling Rate Reconstruction* Technique to reconstruct the signal. As the reducing sample, the signal is still rough and under-sampled. Then, Vi-Liquid utilizes the OMP algorithm to solve the pseudo-inverse matrix and converts the rough signal to the sparse domain.

Interference Cancellation Module: Vi-Liquid will utilize the rough signal obtained from the Signal Reconstruction Module to compare it with the recorded volume magnitude spectrum, and then judge by the threshold to get the liquid volume. Next, Vi-Liquid uses the volume weighting vector to eliminate the sparse signal volume interference. After that, Vi-Liquid combats the straight path interference by subtracting the the Standard Straight Path Interference (SSPI).

Viscosity Measurement Module: Vi-Liquid needs to convert the volume-eliminated sparse signal into a time-domain signal. Then, Vi-Liquid combines the decaying factor, amplitude and other known parameters to calculate viscosity.

5 SYSTEM DESIGN OF VI-LIQUID

This section illustrates the proposed solutions to the transmitter, propagation, and receiver side challenges when realizing the viscosity measurement on the smartphone.

5.1 Vibro-motor Selection

In the previous section, we theoretically demonstrated the feasibility of estimating the viscosity of a liquid using vibration. Nevertheless, mobile phones utilize diverse vibration motors. In our pilot study, we found that not all the vibro-motor are applicable for the viscosity measurement using the vibration model we build in Section 2. According to the model, the vibro-motor should generate the shear strength on the liquid. Our implementation adopted the Linear Resonant Actuator(LRA) to generate the vibration, which is available for multiple commercial mobile phone including iPhone 7, 7P, 8, 8P, X and XR. However, because of built-in system protection in iOS, the motor can only vibrate continuously for 0.5 seconds. and then the motor vibration is forcibly paused by the phone for at least 0.25 s.

5.2 Mobile Phone Placement Selection

In the detection procession, we need an appropriate place to ensure that the vibration is efficient. We designed the experiment to find out the proper position. We set the phone's initial position of the experiments when the phone's home button's midpoint and the edge of the container card slot coincide, as shown in Figure 12. This position can ensure the container's balance because continuing shifting to the left will cause the container to tilt due to beyond border of the phone's centre gravity and keep the motor at the bottom of the phone within the range of action. We shifted the phone to the right to detect the changes caused by the phone offset by 3mm and 6mm. We used the signal when there was no vibration as the noise, and calculated the signal-to-noise ratio received by the accelerometer at different positions. According to the amplitude value curve and the signal-to-noise ratio curve in Figure 13, we

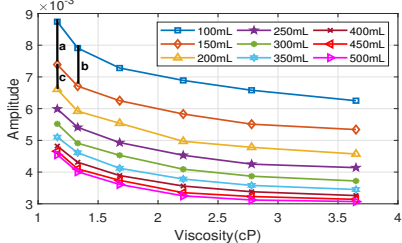


Figure 7: The attenuation of volume to viscosity is not proportional.

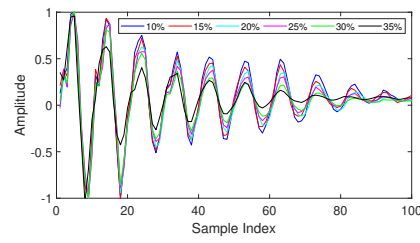


Figure 8: Decaying-state of solution of different mass concentration after the motor stops moving.

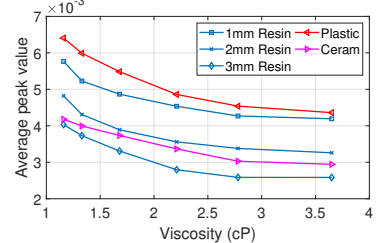


Figure 9: The average peak value affected by the container's material and thickness.

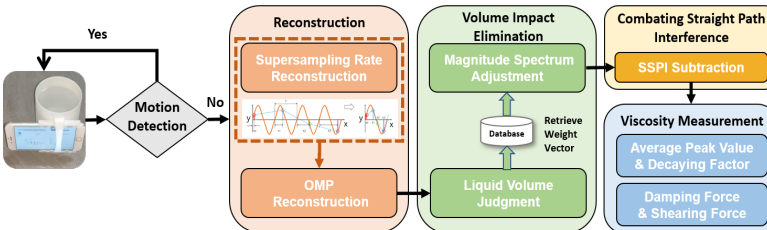


Figure 10: The workflow of Vi-Liquid.

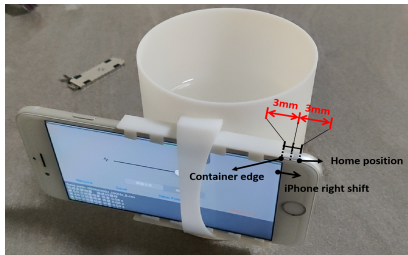


Figure 12: The initial position and direction of phone placement.

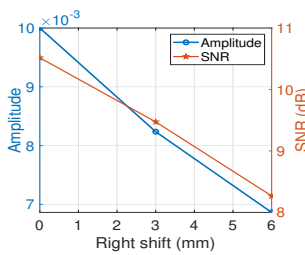


Figure 13: The effect of amplitude and SNR in different phone placement.

found that when the mobile phone shifts to the right, it will cause the signal-to-noise ratio to drop. Also, the reduction of the measurement amplitude will reduce the viscosity range of detection. Therefore, we chose the position where the midpoint of the Home button overlap with the best signal-to-noise ratio coincides with the card slot's edge. Note that the vibro-motor is under the Home button of the mobile phone. As long as the mobile phone position shifts, the motor's torque force will be changed, thereby affecting detection accuracy. Therefore, we strictly controlled the placement of the mobile phone during the experiments.

5.3 Combating Straight Path Interference

In Section 3, we built an external circuit for feasibility study, which means that we did not consider the straight path interference. The straight path interference implies that the vibro-motor's vibration transmits directly to the internal accelerometer rather than passing through the target liquid. The energy of straight path interference is significant, and the useful signal energy related to the viscosity is much lower than the interference. Therefore, we need to remove the straight path signal.

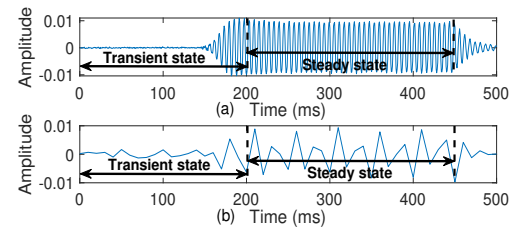


Figure 11: The transient signal in different sampling rate. (a) 1600Hz. (b) 100Hz.

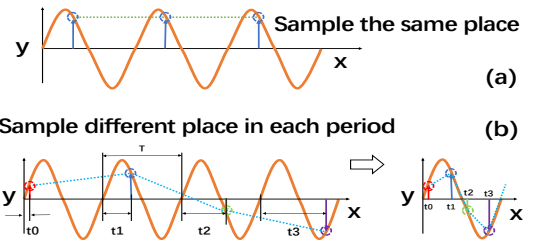


Figure 14: The solution of undersample rate. (a) Same sampling rate as the signal frequency. (b) The solution schematic of undersample rate.

In order to understand the straight path interference, we need to use a high-precision accelerometer to sample the signal for analysis. We replaced the accelerometer chip in the iPhone 7 with a stand-alone accelerometer (BMI160) to record the vibration of straight path interference at 1600Hz sampling rate. It should notice that BMI160 is also used to assist in solving the observation matrix. Through the signal collected by BMI160, as shown in Figure 11, we can observe a transient signal in the first 200 ms. Therefore, to eliminate the dirty signal in each detection, we will remove the first 200 ms transient signal.

What's more, we used a titration butterfly clip to suspend the phone in the air and record the vibration signal, because the soft contact points on the clip can absorb the vibration signal and prevent the reflection. We recorded the 300 ms steady-state vibration time-domain signal in 30 experiments and then performed a short-time fast Fourier transform with six 50 ms width segmented signals. We recorded the amplitude-frequency value of each segment and averaged the mode of each frequency point. These values will keep as the Standard Straight Path Interference (SSPI). Since the straight path's interference occupies the majority of signal energy, we have to scale the SSPI in the signal's frequency domain with interference.

To eliminate interference, we subtract SSPI from the frequency domain of the segmented signals reconstructed by SRR and OMPR. After restoring the processed signal to the time domain utilizing the inverse Fourier transform, we will get the clean signal.

5.4 Supersampling Rate Reconstruction (SRR)

The accelerometer in iPhone 7 supports the sampling rate up to 1600 Hz. Still, the maximum sampling rate is only 100 Hz through API due to the protection of iOS, which is much less than the vibration frequency of vibro-motor at around 167 Hz. According to the *Nyquist Sampling Law*, the low sampling rate results in the distortion of vibration waveform in the time-domain. The measurement error will increase because we apply the amplitude peak to estimate the parameters (see Section 2).

Because to realize this supersampling reconstruction method, the signal needs to have sufficient stability. To verify whether the signal stability, we put the two different resolution signals from Figure 11, into the same time axis. By shifting the signal, we minimized the sum of variances of the corresponding points. We compared two signals, only 1.42% variance between them. Therefore, it is feasible to reconstruct the signal using the basic idea above.

Basic idea of SRR. To solve the low sampling rate problem, we apply the *Supersampling Rate Reconstruction*. As shown in Figure 14(a), when given a stable periodic signal, we might sample the same value if the sampling rate is too low and can not record the entire signal. If we can sample at a distinct time point in each period (e.g., start sampling after t_0, t_1, t_2 , and t_3 in Figure 14(b)) and record the timestamp, there will be plenty of sample points after several periods. Then we combine these sample points into one period and sort them by the timestamps. Finally, the re-ordered signal is comparable to the signal sampled at a high sampling rate. Above this is the basic idea of *Supersampling Rate Reconstruction*.

Explore reasonable sampling intervals. When we perform the discrete Fourier transform on a signal, we will get

$$X(e^{j\omega}) = \sum_{n=1}^N x[t_n] e^{-j\omega t_n} \quad (9)$$

where t_n is the sampling time. When we substitute the t_n with any random number into the above formula, we can observe that the discrete Fourier transform will introduce random noise in the frequency domain, as shown in Figure 15(b). Then, we assume that time t_n obeys a uniform distribution, and its probability density distribution function is $p(t) = \frac{1}{T_{\max}}, t \in [0, T_{\max}]$ and $t \in [0, T_{\max}]$. We will get the spectrum expectations as:

$$\begin{aligned} E[X(e^{j\omega})] &= \frac{1}{T_{\max}} \sum_{n=1}^N \int_0^{T_{\max}} x[t_n] e^{-j\omega t_n} dt_n \\ &= \frac{N}{T_{\max}} \int_0^{T_{\max}} x[t] e^{-j\omega t} dt = \frac{N}{T_{\max}} X(j\omega) \end{aligned} \quad (10)$$

As shown in Figure 15, (a) is a 100Hz non-uniformly spaced signal with 1000 Hz sample rate. If t_n obeys uniform distribution, the magnitude spectrum of uniform sampling is shown in Figure 15(c).

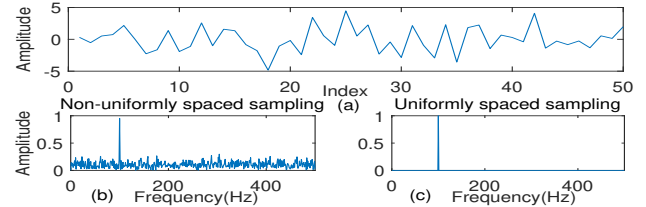


Figure 15: The original signal and the magnitude spectrum obtained by sampling the original signal at different time intervals.

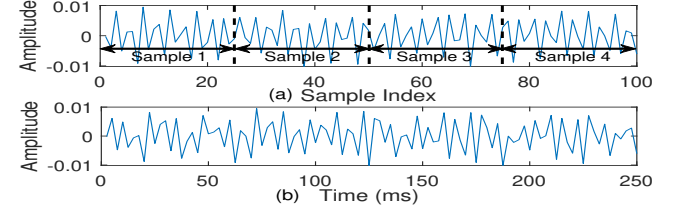


Figure 16: We restore the vibration signal with Supersampling Rate Reconstruction.

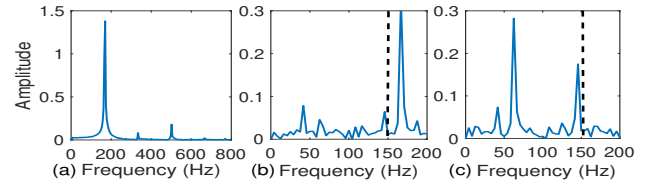


Figure 17: The amplitude-frequency curve of the vibration signal. (a) The original signal received by the BMI160. (b) Correctly re-ordered signal. (c) Incorrectly re-ordered signal.

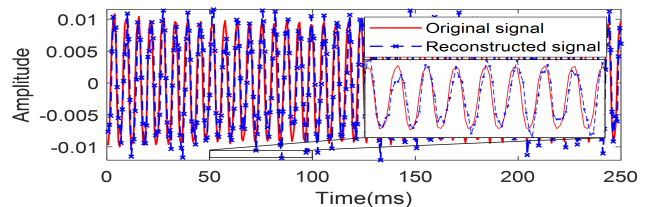


Figure 18: A comparison of the reconstructed signal sampled by 4s and the original signal.

In the practical setting, a cycle composes of 0.5 s active vibration and a pause last for $0.5 s + t_{\text{wait}} \times n_{th}$ cycle.

During the whole process, the accelerometer should keep sampling. After n cycles of sampling, we can achieve SRR for the signal reconstruction.

As shown in Figure 16(a), the under-sampled signal with 100 Hz sampling rate is considerably distorted. We set t_{wait} to be 2.5 ms, apply SRR for four cycles, and get the reconstructed signals as shown in Figure 16(b).

Explore reasonable re-ordered signal. Through observation, we found that when the mobile phone starts the motor, the electrical level is random(0 or 1), which may cause the critical problem -

re-order the signal by inconsistent vibration directions. Because to re-order the n sets of randomness direction signals, it will produce 2^n combinations. If we do not make corrections, this will affect the accuracy of the re-ordered signal. We observed 50 reconstructed signal samples and compared the frequency spectrum of the re-ordered signal. In most cases, as Figure 17 shows, we found that the correctly re-ordered signals have different proportional relations between the frequency domain's peak values. The highest peak in the correctly re-ordered signals will much higher than the other peak values, significantly more than two times larger than the second one.

What's more, the highest peak locate at the position around vibration frequency - greater than 150 Hz. It is because no matter how we re-ordered signal, the total power of the signal is consistent. However, the wrong re-ordered signal brings various frequencies of noise signals, distributing the total signal power. Secondly, there is a certain probability that the wrong re-ordered will lead to most of the points on the coaxial Y axis, which will bring energy-intensive low-frequency signals (because the wave fluctuation becomes slow down). Therefore, we set up a threshold (two times more distinguished than others compare with the highest peak), and in which larger than 150Hz in frequency - to make a simple judgment to select the appropriate re-ordered signal result.

5.5 Orthogonal Matching Pursuit based Reconstruction (OMPR)

Using the peak amplitude as a critical indicator will bring a severe shortcoming that requires a high sampling rate for signal acquisition. Because when the sampling rate is too low, it is difficult to obtain accurate peak amplitude information at the sampling point. If SRR is used to recover a signal with a high sampling rate, it will take much time. Therefore, we build based on SRR and further use OMPR to enhance signal resolution for improving efficiency.

We can confirm from the previous experiments vibration signals in the frequency domain shown in Figure 17, the signal has fewer characteristic frequency points (non-zero points). We set up a threshold of 0.03 to remove the frequency points with inconspicuous features. At this time, the signal is sparse in the frequency domain. The original signal can reconstruct The signal characterizing with sparsity through a nonlinear reconstruction algorithm [7].

Because the high-sampled signal undergoes sampling matrix conversion and finally forms a low-sampled signal. The low sampling signal can express as

$$y = \varphi x \quad (11)$$

where $x \in R^n$ and $\varphi \in R^{m \times n}$ is the the high sampling rate signal and sampling matrix. $y \in R^m$, $m < n$. We know that the original high-sampling rate signal has sparsity in the discrete Fourier transform domain, and the sparsified signal can be expressed as f .

$$y = \varphi \phi f \quad (12)$$

where ϕ is an inverse transform operator. For the sake of simplicity, we represent $\varphi \phi$ as the observation matrix T . Therefore, we only need to find the smallest zero norm f that satisfies the condition of y . At this time, the 0-norm problem can be transformed into a 1-norm problem[7].

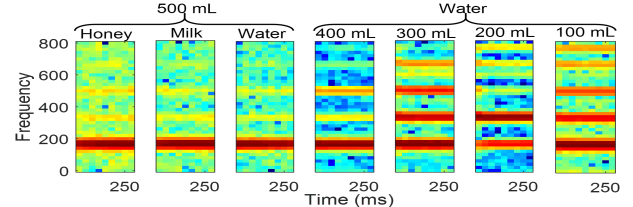


Figure 19: The magnitude spectrum of liquids with different viscosities and different volumes.

To obtain a suitable observation matrix T , we conduct the following experiment. We pour the sucrose solute in different mass (from 1 g to 500 g in a step of 1 g) into the water from 500 liquid samples. For all the samples, we record the vibration signal generated by vibro-motor using a stand-alone accelerometer (sampling at 1600Hz) and built-in accelerometer in the smartphone (sampling at 100Hz), respectively.

We reconstruct the low sampling rate signals to 167 Hz using SRR and denote the reconstructed signal as y_i . We consider high sampling rate signals as the original signal, and denote it as f_i . We substitute f_i and y_i into Equation 12 and obtain a multi-dimensional non-homogeneous linear equation. By solving the equation, we can get the observation matrix T .

Now, we know the observation matrix T . However, to complete the reconstruction, there is one last problem to be solved. Although we can get y during the measurement, it is a very complicated mathematical problem to solve the inverse matrix of the observation matrix T . Therefore, we need to use the pseudo-inverse matrix instead of the real value to solve. Specifically, we use the famous orthogonal matching pursuit (OMP) algorithm [34] to solve the inverse matrix. The OMP algorithm calculates the contribution values of the observation matrix T and y . It continuously updates the residual error for iterative convergence, and finally obtains the sparse signal f from the original signal. As shown in Figure 18, we further restore the signal reconstructed by SRR to 1600 Hz using the OMPR. Note that, if we use OMPR directly because the sampling rate of 100 Hz on the mobile phone is too low, the restored results are not good.

5.6 Combating Volume Change Impact

Recalling the observation in Section 3.2, the liquid's volume change with the same viscosity causes different vibration readings. Suppose we measure the liquid viscosity with varying vibration readings using our proposed model. We will get different results if we measure the liquid viscosity with varying vibration readings using our proposed model, i.e., one kind of liquid in different volumes will have different viscosity, which is not tally with the fact.

Volume Weight Vector. In the experiment of Section 3.2, we found that if the container contains different volumes of liquid, then the steady-state vibration signal we receive will have a different amplitude-frequency curve. It is worth noting that the various volumes of amplitude-frequency curves are quite different. As shown in Figure 19, the different viscosities liquids with the same volume showed similar magnitude spectrums on the left half. In contrast, the different volumes with the same viscosity showed diverse magnitude spectrums. We can observe that the volume influenced the

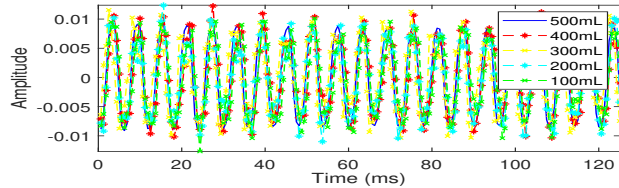


Figure 20: Use super-resolution to reconstruct signals for different volumes. magnitude spectrum's amplitude-frequency curve(the value of each column in the subfigure), but it is independent with the liquid viscosity. This results can be explained using our common sense, for example, tapping a tumbler with various volumes of liquid will hear different sounds. The main reason is that the liquid volumes will change the natural frequency of the entire system. Our idea is to weight the vibration signal results from different liquid volume and unify their amplitude to eliminate the volume impact. We use the 500 ml liquid as the reference liquid. In the magnitude spectrum, the amplitude of reference liquid at frequency bin i is a^{ref}_i .

The volume weight vector W_{volume} is defined as:

$$W_{volume} = \left[\frac{a^{vol}_1}{a^{ref}_1}, \dots, \frac{a^{vol}_i}{a^{ref}_i}, \dots, \frac{a^{vol}_{800Hz}}{a^{ref}_{800Hz}} \right] \quad (13)$$

where a^{vol}_i indicates the amplitude at frequency bin i in the magnitude spectrum of a certain volume liquids.

Liquid Volume Estimation. However, we need to obtain the prior value of the liquid volume first and then apply the corresponding volume weight vector to the signal.

The container can be simplified as a cavity in the physical model. According to the Helmholtz vibration theory [12], the relationship between the resonance frequency f_r and the liquid volume V_l can express as:

$$f_r = \frac{v}{2\pi} \sqrt{\frac{C}{V_l}} \quad (14)$$

where v is the propagation speed of vibration, V_l is the liquid volume, and C is the conductivity of the container. As the liquid volume increases, the resonance frequency decreases. Therefore, we can now infer the liquid volume based on the frequency information. Specifically, we collected the signal for 4 seconds to reconstruct the vibration signal by SSR and OMPR, then calculated the magnitude spectrum based on this signal and obtained frequency deviation information. The relationship between the frequency and liquid volume can be learned and stored in the database in advance. Therefore, we can now get the liquid volume V_l by matching the samples in the database.

Combining the method in the previous section, we eliminate the interference caused by different volumes. As shown in Figure 20, using super-resolution reconstruction signals for different volumes, the curves obtained are very similar, and the residual of least square is only 0.023.

5.7 System Calibration

Considering the system's errors, which may be caused by slight differences in mobile phones or subtle changes in the container's wall material, we found it necessary to calibrate before using the system. Note that the impetus of different mobile phone motors varies. Therefore, we compared the four types of mobile phone,

Table 1: Measuring viscosity for various liquids with Vi-Liquid and viscometer (\pm shows std. GT for ground truth.)

Liquid	β	$f_{\tau(N)}$	Vi-Liquid(cP)	GT(cP)	Error(%)
5%salt solution	0.8775	0.0134	1.03 ± 0.019	1.00	3.00
10%salt solution	0.8757	0.0142	1.09 ± 0.019	1.07	1.87
5%sucrose solution	0.8760	0.0140	1.08 ± 0.025	1.06	1.89
10%sucrose solution	0.8745	0.0155	1.19 ± 0.031	1.16	2.59
Coffee(10g sugar)	1.3770	0.0498	3.83 ± 0.194	3.78	1.32
Coffee(15g sugar)	1.4392	0.0525	4.04 ± 0.094	3.94	2.53
Coffee(sugar-free)	1.3566	0.0489	3.76 ± 0.169	3.65	3.01
Whole milk	0.8980	0.0218	1.68 ± 0.119	1.75	4.00
Skim milk	0.8745	0.0156	1.20 ± 0.075	1.26	4.76
Yogurt	55.545	2.0887	159.14 ± 4.800	152.45	4.39
Beer	0.8748	0.0148	1.14 ± 0.013	1.11	2.70
Chinese liquor	0.8745	0.0155	1.19 ± 0.031	1.23	3.25
Coca-Cola	0.8747	0.0149	1.15 ± 0.019	1.13	1.77
Pepsi-Cola	0.8745	0.0159	1.22 ± 0.013	1.24	1.61
Chocolate liquor	14.888	0.5625	43.28 ± 0.756	40.06	3.22
Honey	1009.8	37.899	2815.28 ± 58.88	3000.12	6.16
Sweet tea	0.8751	0.0166	1.28 ± 0.025	1.32	3.03
Green tea	0.8782	0.0131	1.01 ± 0.019	1.03	1.94
Pineapple juice	33.245	1.2518	96.29 ± 3.78	100.02	3.72
Tomato juice	28.015	1.0555	81.19 ± 1.45	79.03	2.73
Vinegar	0.9393	0.0261	2.01 ± 0.056	2.05	1.95
Soy sauce	0.9799	0.0292	2.25 ± 0.113	2.18	3.37
Soya bean oil	21.145	0.7976	61.35 ± 0.756	59.29	3.47
Vegetable oil	10.214	0.3870	29.77 ± 0.644	30.94	3.78
Lard oil	19.233	0.7258	55.83 ± 0.756	53.18	4.98
Oil(light)	39.047	1.4695	113.04 ± 1.906	108.49	4.19
Oil(heavy)	231.24	8.6821	684.31 ± 3.325	658.12	3.98
Disinfectant alcohol	0.8809	0.0189	1.45 ± 0.075	1.42	2.11
Glycerol	273.09	10.253	788.67 ± 4.800	800.45	1.47
Laundry detergent	70.319	2.6432	203.32 ± 2.331	201.05	1.13

and observed the vibration signal. However, the curve slope of the liquid was independent of the impetus. We tested four common liquids with known viscosity (η_1, η_2, η_3 and η_4). We selected standard liquid distilled water, 5%, 10% and 20% pure sucrose solution. Each liquid had four volumes, ranging from 100-500ml, and a 100ml gap between each calibration. We input these four viscosities into the system. According to Equation 5, we could complete the calibration of the parameters k, m, f_0 and $S_0 \frac{v}{x}$ by solving the following Simultaneous Equations:

$$\begin{cases} \eta_1 = E(k, m, f_0, S_0 \frac{v}{x}) \\ \eta_2 = E(k, m, f_0, S_0 \frac{v}{x}) \\ \eta_3 = E(k, m, f_0, S_0 \frac{v}{x}) \\ \eta_4 = E(k, m, f_0, S_0 \frac{v}{x}) \end{cases} \quad (15)$$

6 SYSTEM EVALUATION

6.1 Experiment Setup

In the following experiments, we deployed the iPhone 7 in the side slot of the 3D-printed container to measure the viscosity, as shown in Figure 1. The vibration frequency of vibro-motor was 167 Hz, and the accelerometer's sampling rate was 100 Hz. The difference in waiting time t_{wait} was 2.5 ms, and we stopped sampling after the motor restarts four times. We utilized viscometer ATAGO – VISCOTM 895 for ground truth measurement. We repeated each measurement for 10 times and obtained the mean value. The rest of the settings was the same as that in the feasibility study.

6.2 Liquid Identification Performance

To verify the effectiveness of our proposed model and techniques, we first used our system to measure the viscosity of 30 kinds of

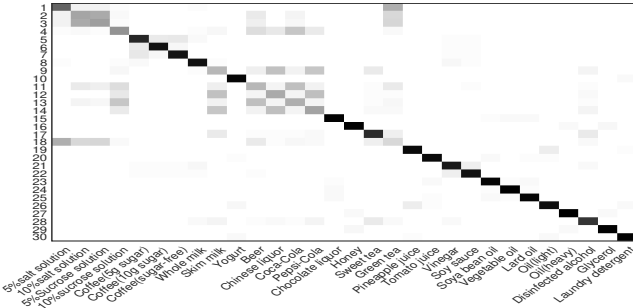


Figure 21: Confusion matrix for liquid identification with estimated viscosity.

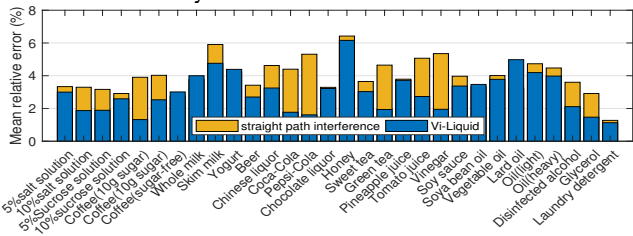


Figure 22: The estimated viscosity errors of the signals with the straight path interference.

liquid (500 mL) and compared the estimated results with the ground truth. As shown in Table 1, the liquids we chose are common in daily life, including beverages with different formulas, such as Coke and Pepsi. We also estimated liquids with different salt, sugar, and fat concentrations. In addition, we selected some readily obtained dangerous liquids as test samples as well.

Baseline accuracy. We report the estimated viscosity for 30 different liquids in Table 1. Through the results, we can notice that Vi-Liquid is effective in measuring viscosity. Comparing to the ground truth, the mean relative error of our system is 2.9%. By taking the estimated viscosity as features, ground truth as labels, we can adopt a simple K-Nearest Neighbors algorithm (K=1) to differentiate those liquids. Figure 21 presents the resulting confusion matrix, which shows an average classification accuracy of 95.47% for 30 kinds of liquids. Evidently, Vi-Liquid can distinguish a large number of liquids correctly, even if they are highly similar, like Coke and Pepsi.

Impact of straight path interference. Due to the straight path interference from the motor to the accelerometer, the low SNR boosts the measurement deviation. In Figure 22, we can see the mean relative error without removing the straight path interference is 3.96% which is much higher than the baseline. This comparison shows the necessity of eliminating the straight path interference.

Impact of sampling rate. The low sampling rate will generate a sampling deviation caused by waves superposition and phase change. It will cause considerable errors in fine-grained analysis. We utilized a signal reconstruction mechanism to restore the under-sampled signal to a high sampling rate and decrease the mean relative error by 1.41%, as shown in Figure 23.

Impact of volume. In this experiment, we measured the viscosity of water, milk, and orange juice in different volumes (i.e., 100 ml,

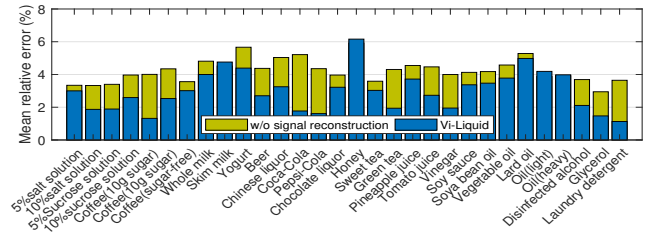


Figure 23: The mean errors of using the original signals to estimate the viscosities.

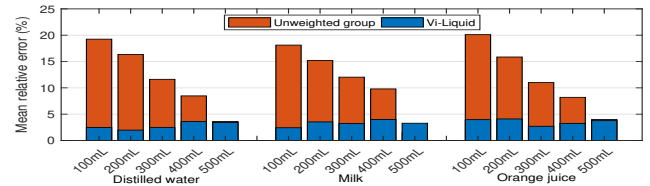


Figure 24: Comparing the changes in viscosity measurement before and after using the volume elimination method.

200 mL, 300 mL, 400 mL, 500 mL) without weighting the signal. We can see from the results shown in Figure 24 that the unweighted group produces large and unacceptable estimation variation and error. After we set the weight based on the analysis of the amplitude-frequency diagram discussed in Section 5.6, we can eliminate the influence results from the volume variation; hence the measured viscosity of the same liquid in different volumes is constant.

6.3 Water Contamination Detection

Drinking non-potable water often results in severe consequences, such as fever, diarrhea, retching, or even death sometimes. The common non-potable water includes tap water, rainwater, puddle water, and water exposed to the air for a long time; they have subtle differences. Tap water always contains organic compounds, heavy metal ions, and residual disinfectant; rainwater carries much atmospheric dust. And puddle water always mixes with large suspended particles. The water exposed for a long time in the air will breed a large number of bacteria and contains unknown secretions.

In this experiment, we aim to validate that our system can distinguish the subtle differences in the above mentioned five water sources by measuring viscosity. The estimated viscosity of the water sources mentioned above demonstrates in Figure 25. The mean relative error is 2.56%, which indicates that if the unknown liquid's viscosity is higher than that of potable water by 0.1 cP, we can be confident that the unknown liquid is non-potable. Among different water sources, distilled water and tap water have the smallest difference in viscosity. Although the difference is only 0.1 cP, it is sufficient for the users to judge if the water has a contamination sign. Therefore, Vi-Liquid can help the area with limited sanitary water facilities detect the water contamination effectively.

6.4 Urine Composition Discrimination

Common causes of kidney disease [12] are bacterial infections, high blood pressure, and diabetes. When kidney disease occurs, glomeruli filter function or renal tubule reabsorption function degrades, causing the uric acid and protein to leak into the urine.

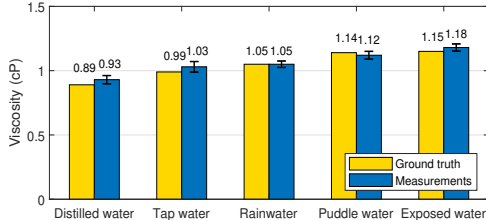


Figure 25: Water contamination detection.

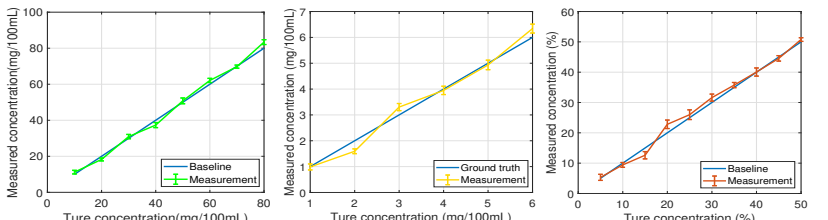


Figure 26: Concentration level estimation based on viscosity.

Therefore, the uric acid and protein concentration in urine is an important indicator of kidney function damage and many other physiological diseases. However, to find out the kidney disease through the general urine test requires patients to go to the hospital themselves. It is inconvenient and prevents many patients from getting timely medical treatment. We hope that Vi-Liquid can help people monitor their uric acid and protein levels in urine at home using just a mobile phone. In this way, people can adjust their physical activity and eating behaviors to avoid the deterioration of the disease, or they can seek a doctor for medical examination in time when the protein levels exceed a safe threshold.

Since it is hard to control urine substances, we synthesized artificial urine by mixing distilled water and quantitative urea (agricultural nitrogen fertilizer) according to the urea content of a healthy person at 38 mg/100mL. We then poured different levels of sodium urate and ovalbumin powder into the artificial urine, respectively, to form the urine sample with different uric acid and protein concentration. Figure 26 gives the urine viscosity level with the increase of uric acid and protein concentration. The mean absolute error is 1.15 mg/100mL for uric acid and 0.20 mg/100mL for protein. Note that the patient typically has the nephritis if the concentration of uric acid is higher than 60 mg/100mL [15] and the complication of microalbuminuria if the concentration of protein is higher than 3 mg/100mL [36].

6.5 Alcohol Concentration Measurement

Ethanol solution is a mixture of ethanol and water. The viscosity of ethanol is higher than water. Intuitively, the viscosity of ethanol solution increases with a higher concentration level of ethanol. With the help of Vi-Liquid for measuring ethanol concentration and volume of alcohol drinks, people can monitor their daily amount of ethanol intake with a mobile phone, thereby avoiding health risks, dangerous driving, and drug toxicity. The relationship between measured viscosity and ethanol concentration is plotted in Figure 26. The result shows that Vi-Liquid can accurately estimate the ethanol concentration with a mean absolute error of 1.38 mass%.

6.6 The Boundary of Measurement

We noticed that Vi-Liquid has a relatively high error of 6.16% when measuring honey of 3000 cP. We speculated that when the viscosity coefficient is higher, the difference in the shearing force generated by the vibrating liquids to the cup wall is more difficult to reflect in the vibration reading. Therefore, in this experiment, we explored the upper boundary for viscosity measurement in Vi-Liquid. We define the available upper boundary as the time when the estimation error exceeds 5%. As shown in Figure 27, honey is a typical liquid that

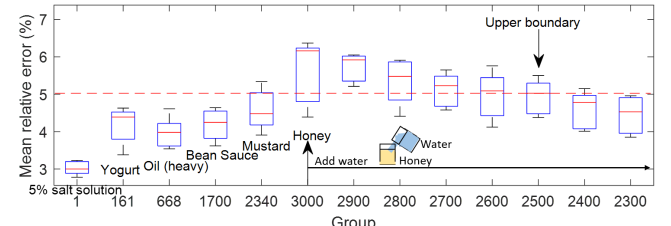


Figure 27: Explore the boundary of viscosity measurement of our system.

exceeds the upper measurement boundary of Vi-Liquid. We diluted the honey with water to reduce its viscosity until the measurement error is near 5%. At this point, we regard that 2500 cP as the upper boundary using Vi-Liquid.

7 RELATED WORK

7.1 Ubiquitous Liquid Testing

Recent research on ubiquitous liquid testing has given a large number of different problem-solving theories and meaningful applications. They mainly lies in two categories, namely RF-based [11, 17, 35, 38] and optical camera based [18, 25, 28, 42].

RF-based systems: The RF-based systems mainly exploits the radio signal propagation characteristic inside the target liquid to identify liquids. TagScan [35] extracts the RSSI and phase change as features from RFID tag reading and classify 10 liquids. Liquid [11] uses two independent ultra-wideband (UWB) units to estimate liquid's actual permittivity, which scales the identification of liquid type to 33. RFIQ [17] and TagTag [38] propose to attach one RFID tag on the target of interest for liquid testing. They achieve the detection of fake alcohol, baby formula adulteration, fake luxury CHANEL perfume and expired milk by comparing with the training set. Mm-Humidity [9] uses millimeter waves to measure the liquid content in the air. However, their approach can not predict the concentration level and requires a complicated setting (i.e., an RFID reader in [35], and a large container in [11]).

Optical and Camera based systems: Thermal infrared sensor, photodiode and visible light camera are widely used as a photodetector to acquire the information about optical absorption or reflection of liquid. It is easy to reveal the liquid property by analyzing the optical spectra. In Nutrilyzer [28], a photoacoustic sensing system was proposed. It leverage the modulated shining light of various wavelength to travel through the liquids and produce unique spectra for characterizing the nutrients and adulterants in liquids. By employing the LEDs and photodiodes, Smart-U [18] is able to recognize food or liquid in the spoon because the diversity of substances

in foods will affect the absorption spectrum. Al-light [25] propose a smart ice cube device equipped with near-infrared and visible LEDs, which can estimate the alcohol concentration level of beverages by utilizing the near-infrared spectrometry principle. However, these proposals rely on the extra specialized device for liquid testing, typically unavailable for general users. On the other hand, Vi-Liquid is a smartphone-based liquid testing system that supports multiple applications simultaneously.

CapCam [42] is the first mobile application that can measure liquid surface tension. It leverages the smartphone's vibro-motor to generate capillary waves on the liquid surface and capture the light pattern on the container's bottom using the flashlight camera. However, it is not able to identify unknown liquids and fail to function in testing opaque liquids. In contrast, Vi-Liquid measures the liquid viscosity coefficient through vibration signals, based on supporting all applications of CapCam [42], it can also identify different liquid types without training.

7.2 Measuring Liquid Viscosity

Liquid viscosity testing is one of the main methods to analyze liquid constituents. For example, soil exudate's viscosity [2] will discover the pollutant components, and blood viscosity detection [33] can determine the content of cholesterol deposits. Earlier works, the capillary viscometer [10], the cylindrical torsional viscometer [6] the falling ball viscosity method [16] calculates the liquid's viscosity from Fluid Mechanics. The cantilever beam liquid analyzer [29, 31] applies a cantilever inserted into the liquid to analyze cantilever shaking. [24] used a 3D printed parallelogram flexure hinge structure and optical fibre to replace the traditional system parts, which improved the invasive method's detection accuracy. However, they all need to use very sophisticated instruments, professional researchers to operate and invasive methods. There are not suitable for general beverage identification, and especially the unhygienic devices may lead to contagion risks.

Employing the ultrasonic waves is a non-invasive way. Ultrasonic waves will generate the surface waves [5] directly correlated with the viscosity of liquids. Moreover, the reflection signal [4] also shows the relationship with viscosity. However, demanding liquids to be exposed to the air limits their application scenarios. The application of the photothermal effect [26] to detect the heat capacity ratio relative to viscosity requires a sophisticated and expensive thermal imager. The Brillouin scattering method [39] utilizing light can quickly obtain the viscosity of the liquid, but the ultra-wide bandwidth spectrum and the precise optical path detection equipment largely increase the detection overhead.

Vi-Liquid only employs a smartphone, a readily accessible device, for the non-intrusive viscosity measurement. The systems can be operated by just a single click of the user. Therefore, Vi-Liquid is more suitable for the user to test the liquid in daily life.

7.3 Vibration-based Applications

Recent years have witnessed the rapid development in vibration-based sensing applications, benefiting from vibration signals' excellent properties. A large variety of novel proposals using vibration signals are presented, ranging from keystroke recognition [8, 19, 23], human activity monitoring [20, 21], user authentication [27, 40, 41],

gesture recognition [22, 37], and nearo-field communication [30]. Because the vibration generator and the receiver (i.e., vibro-motor and IMU) is universally embedded in wearables and mobile phone, it is convenient for the researchers to leverage vibration signals for mobile computing. Oinput [19] and VibID [41] leverage passive and active vibration for identification, respectively. TouchPass[40] builds a behavior-irrelevant on-touch user authentication system on smartphones.

Different from these work, Vi-Liquid extends the kinematics equation of single-degree-of-freedom and combines it with the viscosity theory to build a liquid viscosity testing system. It can effectively identify unknown liquid, detect water contamination, monitor alcohol intake, and measure the uric acid and protein concentration in urine.

8 CONCLUSION AND FUTURE WORK

This paper proposes Vi-Liquid, a liquid testing system that can accurately measure the liquid viscosity using vibration signals on smartphones. We establish a novel calculation model that links vibration with viscosity and validate the feasibility on a smartphone. To break the system restriction, we found the proper *Supersampling Rate Reconstruction* and employ OMP reconstruction to restore the undersampled signal. Further, we cancel the straight path interference and volume change impact to improve the system performance. Our comprehensive experiments show that Vi-Liquid can successfully identify 30 kinds of unknown liquids, detect the water contamination, monitor the alcohol intake, measure the concentration level of uric acid and protein in the urine. We envision that Vi-Liquid can serve as a satisfactory assistant for ubiquitous liquid testing in many realistic application scenarios.

However, as a proof-of-concept prototype for liquid viscosity measurement, Vi-Liquid still has some limitations to be addressed in our future work:

Container Types: In this paper, we attach the smartphone to the wall of a 3D-printed container to measure the viscosity. However, in practical usage, the user would like to test the liquids in different containers without attaching the smartphone on the sidewall.

Temperature: According to the viscosity theory, the higher the temperature, the lower the liquid viscosity. For example, the viscosity of water at 20°C is 1 cP, and it will drop to 0.8 cP at 30°C. Therefore, we need to design a novel calibration scheme based on the relationship between temperature and viscosity.

Complex component analysis: If the liquid contains only one molecular component, it can be easily distinguished by viscosity. When the liquid composition is too complex, the interaction force between various molecules is difficult to predict with only a viscosity model. In the future, we will combine with other liquid properties (e.g., density, surface tension, and permittivity) to improve the liquid testing ability on smartphones.

ACKNOWLEDGMENTS

This research was supported in part by the China NSFC Grant (U2001207, 61872248), Guangdong NSF 2017A030312008, Shenzhen Science and Technology Foundation (No. ZDSYS20190902092853047), the Project of DEGP (No.2019KCXTD005), the Guangdong "Pearl River Talent Recruitment Program" under Grant 2019ZT08X603,

Guangdong Science and Technology Foundation (2019B111103001, 2019B020209001), the China NSFC 61872246, Guangdong Special Support Program. Kaishun Wu is the corresponding author.

REFERENCES

- [1] 2020. Apple Inc.CMMotionActivityManager. <https://developer.apple.com/documentation/coremotion/cmmotionactivitymanager>.
- [2] INyoman Aribudiman. 2019. Seepage in soil from the difference of water viscosity using Geo-studio SEEP/W program. *International research journal of engineering, IT & scientific research* 5, 1 (2019), 15–26. <https://doi.org/10.21744/irjeis.v5n1.586>
- [3] Ralph Alger Bagnold. 1954. Experiments on a gravity-free dispersion of large solid spheres in a Newtonian fluid under shear. *Proceedings of the Royal Society of London. Series A, Mathematical and Physical Sciences* 225, 1160 (1954), 49–63. <https://doi.org/10.1098/rspa.1954.0186>
- [4] James D Baird. 1971. Noncontact ultrasonic interface viscosity and percent solid detecting device.
- [5] D. Beyssen, L. Le Brizoual, O. Elmazria, and P. Alnot. 2005. Surface acoustic wave microfluidic device. *Proceedings - IEEE Ultrasonics Symposium* 2, 1-2 (2005), 1028–1031. <https://doi.org/10.1109/ULTSYM.2005.1603026>
- [6] C. Blom and J. Mellema. 1984. Torsion pendula with electromagnetic drive and detection system for measuring the complex shear modulus of liquids in the frequency range 80–2500 Hz. *Rheologica Acta* 23, 1 (1984), 98–105. <https://doi.org/10.1007/BF01333881>
- [7] E.J. Candès and M.B. Wakin. 2008. An Introduction To Compressive Sampling. *IEEE Signal Processing Magazine* 25, 2 (2008), 21–30. <https://doi.org/10.1109/msp.2007.914731>
- [8] Wenqiang Chen, Lin Chen, Yandao Huang, Xinyu Zhang, Lu Wang, Rukhsana Ruby, and Kaishun Wu. 2019. Taprint: Secure Text Input for Commodity Smart Wristbands. In *The 25th Annual International Conference on Mobile Computing and Networking* (Los Cabos, Mexico) (*MobiCom '19*). Association for Computing Machinery, New York, NY, USA, Article 17, 16 pages. <https://doi.org/10.1145/330061.3300124>
- [9] Q. Dai, Y. Huang, L. Wang, R. Ruby, and K. Wu. 2018. mm- Humidity: Fine-Grained Humidity Sensing with Millimeter Wave Signals. In *2018 IEEE 24th International Conference on Parallel and Distributed Systems (ICPADS)*. 204–211. <https://doi.org/10.1109/PADSW.2018.8644907>
- [10] Juan de Vicente, Modesto T. López-López, Juan D. Durán, and Fernando González-Caballero. 2004. Shear flow behavior of confined magnetorheological fluids at low magnetic field strengths. *Rheologica Acta* 44, 1 (2004), 94–103. <https://doi.org/10.1007/s00397-004-0383-6>
- [11] Ashutosh Dhekne, Mahanth Gowda, Yixuan Zhao, Haitham Hassanieh, and Romit Roy Choudhury. 2018. LiquID: A wireless liquid identifier. In *MobiSys 2018 - Proceedings of the 16th ACM International Conference on Mobile Systems, Applications, and Services*. 442–454. <https://doi.org/10.1145/3210240.3210345>
- [12] Simon J Estéve and Marty E Johnson. 2002. Reduction of sound transmission into a circular cylindrical shell using distributed vibration absorbers and Helmholtz resonators. *The Journal of the Acoustical Society of America* 112, 6 (2002), 2840–2848.
- [13] Henry Eyring. 2014. The Activated Complex in Chemical Reactions. *Source Book in Chemistry, 1900–1950* 3, 2 (2014), 107–115. <https://doi.org/10.4159/harvard.9780674366701.c74>
- [14] V. C. A. Ferraro, Sydney Chapman, and T. G. Cowling. 1954. *The Mathematical Theory of Non-Uniform Gases. An Account of the Kinetic Theory of Viscosity, Thermal Conduction, and Diffusion in Gases*. Vol. 38. Cambridge university press. 63 pages. <https://doi.org/10.2307/3609795>
- [15] Margit Fröhlich, Armin Imhof, Gabriele Berg, Winston L Hutchinson, Mark B Pepys, HEIN Boeing, Rainer Muche, Hermann Brenner, and Wolfgang Koenig. 2000. Association between C-reactive protein and features of the metabolic syndrome: a population-based study. *Diabetes care* 23, 12 (2000), 1835–1839.
- [16] Moshe Gottlieb. 1979. Zero-shear-rate viscosity measurements for polymer solutions by falling ball viscometry. *Journal of Non-Newtonian Fluid Mechanics* 6, 2 (1979), 97–109. [https://doi.org/10.1016/0377-0257\(79\)87008-1](https://doi.org/10.1016/0377-0257(79)87008-1)
- [17] Unsoo Ha, Yunfei Ma, Zexuan Zhong, Tzu Ming Hsu, and Fadel Adib. 2018. Learning food quality and safety from wireless stickers. In *HotNets 2018 - Proceedings of the 2018 ACM Workshop on Hot Topics in Networks*. 106–112. <https://doi.org/10.1145/3286062.3286078>
- [18] Qianyi Huang, Zhice Yang, and Qian Zhang. 2018. Smart-U: Smart Utensils Know what You Eat. In *Proceedings - IEEE INFOCOM*, Vol. 2018-April. IEEE, 1439–1447. <https://doi.org/10.1109/INFOCOM.2018.8486266>
- [19] Yongzhi Huang, Shaotian Cai, Lu Wang, and Kaishun Wu. 2019. Oinput: A Bone-Conductive QWERTY Keyboard Recognition for Wearable Device. In *Proceedings of the International Conference on Parallel and Distributed Systems - ICPADS*, Vol. 2018-December. IEEE, 946–953. <https://doi.org/10.1109/PADSW.2018.8644590>
- [20] Y. Huang, W. Chen, H. Chen, L. Wang, and K. Wu. 2019. G-Fall: Device-free and Training-free Fall Detection with Geophones. In *2019 16th Annual IEEE International Conference on Sensing, Communication, and Networking (SECON)*. 1–9.
- [21] Zhenhua Jia, Amelie Bonde, Sugang Li, Chenren Xu, Jingxian Wang, Yanyong Zhang, Richard E. Howard, and Pei Zhang. 2017. Monitoring a Person's Heart Rate and Respiratory Rate on a Shared Bed Using Geophones. In *Proceedings of the 15th ACM Conference on Embedded Network Sensor Systems* (Delft, Netherlands) (*SenSys '17*). Association for Computing Machinery, New York, NY, USA, Article 6, 14 pages. <https://doi.org/10.1145/3131672.3131679>
- [22] Gierad Laput, Robert Xiao, and Chris Harrison. 2016. ViBand: High-Fidelity Bio-Acoustic Sensing Using Commodity Smartwatch Accelerometers. In *Proceedings of the 29th Annual Symposium on User Interface Software and Technology* (Tokyo, Japan) (*UIST '16*). Association for Computing Machinery, New York, NY, USA, 321–333. <https://doi.org/10.1145/2984511.2984582>
- [23] Jian Liu, Yingying Chen, Marco Gruteser, and Yan Wang. 2017. VibSense: Sensing Touches on Ubiquitous Surfaces through Vibration. In *2017 14th Annual IEEE International Conference on Sensing, Communication, and Networking, SECON 2017*. IEEE, 1–9. <https://doi.org/10.1109/SAHCN.2017.7964907>
- [24] Jinyu Ma, Xinjing Huang, Hyungdae Bae, Yelong Zheng, Cong Liu, Meirong Zhao, and Miao Yu. 2016. Liquid viscosity measurement using a vibrating flexure hinged structure and a fiber-optic sensor. *IEEE Sensors Journal* 16, 13 (2016), 5249–5258.
- [25] Hidenori Matsui, Takahiro Hashizume, and Koji Yatani. 2018. Al-light: An Alcohol-Sensing Smart Ice Cube. *Proceedings of the ACM on Interactive, Mobile, Wearable and Ubiquitous Technologies* 2 (09 2018), 1–20. <https://doi.org/10.1145/3264936>
- [26] Masahiro Motosuke, Jun Shimakawa, Dai Akutsu, and Shinji Honami. 2010. Noncontact manipulation of microflow by photothermal control of viscous force. *International Journal of Heat and Fluid Flow* 31, 6 (2010), 1005–1011. <https://doi.org/10.1016/j.ijheatfluidflow.2010.05.005>
- [27] Shijia Pan, Tong Yu, Mostafa Mirshekari, Jonathon Fagert, Amelie Bonde, Ole Mengshoel, Hae Noh, and Pei Zhang. 2017. FootprintID: Indoor Pedestrian Identification through Ambient Structural Vibration Sensing. *Proceedings of the ACM on Interactive, Mobile, Wearable and Ubiquitous Technologies* 1 (09 2017), 1–31. <https://doi.org/10.1145/3130954>
- [28] Tauhidur Rahman, Alexander T. Adams, Perry Schein, Aadhar Jain, David Erickson, and Tanzeem Choudhury. 2016. Nutrilyzer: A mobile system for characterizing liquid food with photoacoustic effect. In *Proceedings of the 14th ACM Conference on Embedded Networked Sensor Systems, SenSys 2016*. 123–136. <https://doi.org/10.1145/2994551.2994572>
- [29] Christian Riesch, Erwin K. Reichel, Franz Keplinger, and Bernhard Jakoby. 2008. Characterizing Vibrating Cantilevers for Liquid Viscosity and Density Sensing. *Journal of Sensors* 2008 (2008), 1–9. <https://doi.org/10.1155/2008/697062>
- [30] Nirupam Roy and Romit Roy Choudhury. 2016. Ripple II: Faster Communication through Physical Vibration. In *Proceedings of the 13th Usenix Conference on Networked Systems Design and Implementation* (Santa Clara, CA) (*NSDI'16*). USENIX Association, USA, 671–684.
- [31] Wan Y. Shih, Xiaoping Li, Huiming Gu, Wei Heng Shih, and Ilhan A. Aksay. 2001. Simultaneous liquid viscosity and density determination with piezoelectric unimorph cantilevers. *Journal of Applied Physics* 89, 2 (2001), 1497–1505. <https://doi.org/10.1063/1.1287606>
- [32] A. E. Simone and L. J. Gibson. 1998. Effects of solid distribution on the stiffness and strength of metallic foams. *Acta Materialia* 46, 6 (1998), 2139–2150. [https://doi.org/10.1016/S1359-6454\(97\)00421-7](https://doi.org/10.1016/S1359-6454(97)00421-7)
- [33] Cesare Tripolino, Concetta Irace, Claudio Carallo, Faustina Barbara Scavelli, and Agostino Gnasso. 2017. Body fat and blood rheology: Evaluation of the association between different adiposity indices and blood viscosity. *Clinical Hemorheology and Microcirculation* 65, 3 (2017), 241–248. <https://doi.org/10.3233/CH-16172>
- [34] Joel A Tropp and Anna C Gilbert. 2007. Signal recovery from random measurements via orthogonal matching pursuit. *IEEE Transactions on information theory* 53, 12 (2007), 4655–4666.
- [35] Ju Wang, Jie Xiong, Xiaojiang Chen, Hongbo Jiang, Rajesh Krishna Balan, and Dingyi Fang. 2017. TagScan: Simultaneous target imaging and material identification with commodity RFID devices. In *Proceedings of the Annual International Conference on Mobile Computing and Networking, MOBICOM*, Vol. Part F131210. 288–300. <https://doi.org/10.1145/3117811.3117830>
- [36] Matthew R Weir. 2007. Microalbuminuria and cardiovascular disease. *Clinical Journal of the American Society of Nephrology* 2, 3 (2007), 581–590.
- [37] Hongyi Wen, Julian Ramos Rojas, and Anind K. Dey. 2016. Serendipity: Finger Gesture Recognition Using an Off-the-Shelf Smartwatch. In *Proceedings of the 2016 CHI Conference on Human Factors in Computing Systems* (San Jose, California, USA) (*CHI '16*). Association for Computing Machinery, New York, NY, USA, 3847–3851. <https://doi.org/10.1145/2858036.2858466>
- [38] Binbin Xie, Jie Xiong, Xiaojiang Chen, Eugene Chai, Liyao Li, Zhenyong Tang, and Dingyi Fang. 2019. Tagtag: Material Sensing with Commodity RFID. In *Proceedings of the 17th Conference on Embedded Networked Sensor Systems (New York, New York) (SenSys '19)*. Association for Computing Machinery, New York, NY, USA, 338–350. <https://doi.org/10.1145/3356250.3360027>

- [39] Jianfeng Xu, Xiaobin Ren, Wenping Gong, Rui Dai, and Dahe Liu. 2003. Measurement of the Bulk Viscosity of Liquid by Brillouin Scattering. *Applied Optics* 42, 33 (2003), 6704. <https://doi.org/10.1364/ao.42.006704>
- [40] Xiangyu Xu, Jiadi Yu, Yingying Chen, Qin Hua, Yanmin Zhu, Yi-Chao Chen, and Minglu Li. 2020. TouchPass: Towards Behavior-Irrelevant on-Touch User Authentication on Smartphones Leveraging Vibrations. In *Proceedings of the 26th Annual International Conference on Mobile Computing and Networking* (London, United Kingdom) (*MobiCom '20*). Association for Computing Machinery, New York, NY, USA, Article 24, 13 pages. <https://doi.org/10.1145/3372224.3380901>
- [41] Lin Yang, Wei Wang, and Qian Zhang. 2016. VibID: User Identification through Bio-Vibrometry. In *2016 15th ACM/IEEE International Conference on Information Processing in Sensor Networks, IPSN 2016 - Proceedings*. IEEE, 1–12. <https://doi.org/10.1109/IPSN.2016.7460725>
- [42] Shichao Yue and Dina Katabi. 2019. Liquid testing with your smartphone. In *MobiSys 2019 - Proceedings of the 17th Annual International Conference on Mobile Systems, Applications, and Services*. 275–286. <https://doi.org/10.1145/3307334.3326078>